AFRL-RX-WP-JA-2015-0209

VARIABLE DEFLECTION RESPONSE OF SENSITIVE CNT-ON-FIBER ARTIFICIAL HAIR SENSORS FROM CNT SYNTHESIS IN HIGH ASPECT RATIO MICROCAVITIES (POSTPRINT)

Jeff Baur
Materials and Manufacturing Directorate, Air Force Research Laboratory

Keith Slinker and Corey Kondash
Universal Technology Corporation

Matthew Maschmann
Mechanical and Aerospace Engineering Department, University of Missouri

Benjamin Severin
Federal Republic of Germany Liaison Office for Defense Material USA/Canada

APRIL 2015
Interim Report

AIR FORCE RESEARCH LABORATORY
MATERIALS AND MANUFACTURING DIRECTORATE
WRIGHT-PATTERSON AIR FORCE BASE OH 45433-7750
AIR FORCE MATERIEL COMMAND
UNITED STATES AIR FORCE

NOTICE AND SIGNATURE PAGE

Using Government drawings, specifications, or other data included in this document for any purpose other than Government procurement does not in any way obligate the U.S. Government. The fact that the Government formulated or supplied the drawings, specifications, or other data does not license the holder or any other person or corporation; or convey any rights or permission to manufacture, use, or sell any patented invention that may relate to them.

Qualified requestors may obtain copies of this report from the Defense Technical Information Center (DTIC) (http://www.dtic.mil).

AFRL-RX-WP-JA-2015-0209 HAS BEEN REVIEWED AND IS APPROVED FOR PUBLICATION IN ACCORDANCE WITH ASSIGNED DISTRIBUTION STATEMENT.

//Signature//

JEFFERY W. BAUR, Project Engineer
Composites Branch
Structural Materials Division

//Signature//

MICHAEL J. KINSELLA, Chief
Composites Branch
Structural Materials Division

//Signature//

ROBERT T. MARSHALL, Deputy Chief
Structural Materials Division
Materials And Manufacturing Directorate

This report is published in the interest of scientific and technical information exchange and its publication does not constitute the Government's approval or disapproval of its ideas or findings.

REPORT DOCUMENTATION PAGE

Form Approved
OMB No. 0704-0188

1. REPORT DATE *(DD-MM-YY)*	2. REPORT TYPE	3. DATES COVERED *(From - To)*
April 2015	Interim	26 April 2012 – 26 March 2015

4. TITLE AND SUBTITLE
VARIABLE DEFLECTION RESPONSE OF SENSITIVE CNT-ON-FIBER ARTIFICIAL HAIR SENSORS FROM CNT SYNTHESIS IN HIGH ASPECT RATIO MICROCAVITIES (POSTPRINT)

5a. CONTRACT NUMBER
FA8650-11-D-5800-0003

5b. GRANT NUMBER

5c. PROGRAM ELEMENT NUMBER
62102F

6. AUTHOR(S)
See back.

5d. PROJECT NUMBER
4347

5e. TASK NUMBER

5f. WORK UNIT NUMBER
X0HA

7. PERFORMING ORGANIZATION NAME(S) AND ADDRESS(ES)
See back.

8. PERFORMING ORGANIZATION REPORT NUMBER

9. SPONSORING/MONITORING AGENCY NAME(S) AND ADDRESS(ES)
Air Force Research Laboratory
Materials and Manufacturing Directorate
Wright-Patterson Air Force Base, OH 45433-7750
Air Force Materiel Command
United States Air Force

10. SPONSORING/MONITORING AGENCY ACRONYM(S)
AFRL/RXCC

11. SPONSORING/MONITORING AGENCY REPORT NUMBER(S)
AFRL-RX-WP-JA-2015-0209

12. DISTRIBUTION/AVAILABILITY STATEMENT
Distribution Statement A. Approved for public release: distribution unlimited.

13. SUPPLEMENTARY NOTES
Article published in *SPIE Vol. 9429, 942917*. © 2015 SPIE. The U.S. Government is joint author of the work and has the right to use, modify, reproduce, release, perform, display or disclose the work. This report contains color. The final publication is available at doi: 10.1117/12.2085568.

14. ABSTRACT

Crickets, locusts, bats, and many other animals detect changes in their environment with distributed arrays of flow sensitive hairs. Here we discuss the fabrication and characterization of a relatively new class of pore-based, artificial hair sensors that take advantage of the mechanical properties of structural microfibers and the electromechanical properties of self-aligned carbon nanotube arrays to rapidly transduce changes in low speed air flow. The radially aligned nanotubes are able to be synthesized along the length of the fibers inside the high aspect ratio cavity between the fiber surface and the wall of a microcapillary pore. The growth self-positions the fibers within the capillary and forms a conductive path between detection electrodes. As the hair is deflected, nanotubes are compressed to produce a typical resistance change of 1-5% per m/s of air speed which we believe are the highest sensitivities reported for air velocities less than 10 m/s. The quasi-static response of the sensors to point loads is compared to that from the distributed loads of air flow. A plane wave tube is used to measure their dynamic response when perturbed at acoustic frequencies. Correlation of the nanotube height profile inside the capillary to a diffusion transport model suggests that the nanotube arrays can be controllably tapered along the fiber. Like their biological counterparts, many applications can be envisioned for artificial hair sensors by tailoring their individual response and incorporating them into arrays for detecting spatio-temporal flow patterns over rigid surfaces such as aircraft.

15. SUBJECT TERMS
artificial hair, flow sensor, carbon nanotube synthesis

16. SECURITY CLASSIFICATION OF:			17. LIMITATION OF ABSTRACT:	18. NUMBER OF PAGES	19a. NAME OF RESPONSIBLE PERSON (Monitor)
a. REPORT	b. ABSTRACT	c. THIS PAGE			Jeffery W. Baur
Unclassified	Unclassified	Unclassified	SAR	17	19b. TELEPHONE NUMBER *(Include Area Code)* (937) 255-9324

REPORT DOCUMENTATION PAGE Cont'd

6. AUTHOR(S)

Jeff Baur - Materials and Manufacturing Directorate, Air Force Research Laboratory
Keith Slinker and Corey Kondash - Universal Technology Corporation
Matthew Maschmann - Mechanical and Aerospace Engineering Department, University of Missouri
Benjamin Severin - Federal Republic of Germany Liaison Office for Defense Material USA/Canada
David Phillips - University of Dayton Research Institute
Benjamin T. Dickinson - Munitions Directorate, Air Force Research Laboratory
Greg Reich - Aerospace Systems Directorate, Air Force Research Laboratory

7. PERFORMING ORGANIZATION NAME(S) AND ADDRESS(ES)

Materials and Manufacturing Directorate, Air Force Research Laboratory, Wright-Patterson Air Force Base, Ohio

Universal Technology Corporation, Beavercreek, Ohio

Mechanical and Aerospace Engineering Department, University of Missouri, Columbia, Missouri

Federal Republic of Germany Liaison Office for Defense Material USA/Canada, Reston, Virginia

University of Dayton Research Institute, Dayton, Ohio

Munitions Directorate, Air Force Research Laboratory, Eglin Air Force Base, Florida

Aerospace Systems Directorate, Air Force Research Laboratory, Wright-Patterson Air Force Base, Ohio

Variable Deflection Response of Sensitive CNT-on-Fiber Artificial Hair Sensors from CNT Synthesis in High Aspect Ratio Microcavities

Keith Slinker[*a,b], Matthew Maschmann[a,b,c], Corey Kondash[a,b], Benjamin Severin[d,f], David Phillips[a,e], Benjamin T. Dickinson[f], Greg Reich[g], Jeff Baur[a]

[a]Materials and Manufacturing Directorate, Air Force Research Laboratory, Wright-Patterson Air Force Base, Ohio, USA; [b]Universal Technology Corporation, Beavercreek, Ohio, USA; [c]Mechanical and Aerospace Engineering Department, University of Missouri, Columbia, Missouri, USA; [d]Federal Republic of Germany Liaison Office for Defense Material USA/Canada, Reston, Virginia, USA; [e]University of Dayton Research Institute, Dayton, Ohio, USA; [f]Munitions Directorate, Air Force Research Laboratory, Eglin Air Force Base, Florida, USA; [g]Aerospace Systems Directorate, Air Force Research Laboratory, Wright-Patterson Air Force Base, Ohio, USA

ABSTRACT

Crickets, locusts, bats, and many other animals detect changes in their environment with distributed arrays of flow-sensitive hairs. Here we discuss the fabrication and characterization of a relatively new class of pore-based, artificial hair sensors that take advantage of the mechanical properties of structural microfibers and the electromechanical properties of self-aligned carbon nanotube arrays to rapidly transduce changes in low speed air flow. The radially aligned nanotubes are able to be synthesized along the length of the fibers inside the high aspect ratio cavity between the fiber surface and the wall of a microcapillary pore. The growth self-positions the fibers within the capillary and forms a conductive path between detection electrodes. As the hair is deflected, nanotubes are compressed to produce a typical resistance change of 1-5% per m/s of air speed which we believe are the highest sensitivities reported for air velocities less than 10 m/s. The quasi-static response of the sensors to point loads is compared to that from the distributed loads of air flow. A plane wave tube is used to measure their dynamic response when perturbed at acoustic frequencies. Correlation of the nanotube height profile inside the capillary to a diffusion transport model suggests that the nanotube arrays can be controllably tapered along the fiber. Like their biological counterparts, many applications can be envisioned for artificial hair sensors by tailoring their individual response and incorporating them into arrays for detecting spatio-temporal flow patterns over rigid surfaces such as aircraft.

Keywords: artificial hair, flow sensor, carbon nanotube synthesis

1. INTRODUCTION

Detection of air flow by hair sensors is inspired by the ability of many animals to detect changes in their environment with distributed arrays of flow-sensitive hairs[1-4]. For example, the locust performs angle of sideslip regulation from hair sensor airflow feedback of flow patterns that evolve over its head[3]. Independent of biological inspiration, engineered angle of attack (AoA) and angle of sideslip (AoS) measurement technologies known as air data systems (ADS) were developed relying on pressure sensor arrays located at the nose of various high speed air and spacecraft[5]. In contrast to pressure sensors, artificial hair sensors are a more information rich source of data because their response is determined from a flow velocity field with both magnitude and direction[6] as opposed to a scalar pressure field with pressure sensor based ADS. Additionally, micro-scale artificial hair sensors are suitable flow sensor candidates for insect to bird scale low-Reynolds-number flyers due to their low power consumption, light weight, high sensitivity, and small footprint. Artificial hair sensors are also plausible technologies for aeronautic applications such as attitude control, heading determination, and self-stabilization[7, 8]. The need is for sensors that can rapidly transduce small temporal changes in air flow into detectable signals with many of such sensors able to easily be distributed over aircraft surfaces for spatial flow pattern detection.

*keith.slinker.ctr@us.af.mil; phone 1 937 904-5705; fax 1 937 656-4706

Bioinspiration, Biomimetics, and Bioreplication 2015, edited by Akhlesh Lakhtakia, Mato Knez, Raúl J. Martín-Palma, Proc. of SPIE Vol. 9429, 942917 · © 2015 SPIE
CCC code: 0277-786X/15/$18 · doi: 10.1117/12.2085568

Carbon nanotubes (CNTs) can be synthesized into self-aligned arrays that can exhibit large piezoresistance in response to compression[9-11], and the synthesis of CNT arrays and their subsequent mechanical, electrical, and thermal properties have been widely studied[12-18]. While there has been significant work on planar arrays and the growth on reinforcement fibers[19, 20], there has been limited work on the synthesis of CNT arrays within confined geometries. Envisioned applications require the growth or placement of the nanotube array within a pore or between two closely spaced planar surfaces, but the high aspect ratio of such geometries could potentially represent a challenge in that the catalyst, carbon source, and synthesis conditions must all be present for robust growth of the self-aligned CNT arrays.

Here we discuss the fabrication and characterization of a relatively new class of pore-based, artificial hair sensors that take advantage of the mechanical properties of structural microfibers and the electromechanical properties of self-aligned carbon nanotube (CNT) arrays to rapidly transduce changes in low speed air flow. We have previously demonstrated sensors of this design to have large sensitivity for air velocities around 1 m s^{-1} in response to quasi-static changes in air flow[21]. A resistance change is detected from compression of the nanotube array by the deflection of the hair, and the nanotubes also serve as the mechanical support for the hair[21, 22]. Here a plane wave tube is used to probe the dynamic response of the hair sensors. The quasi-static electromechanical response of the sensors to point loads are compared to the distributed load response to air flow. The role of the nanotubes in the response of the sensors in both cases is investigated.

The nanotubes are able to be synthesized down the length of the fibers inside the high aspect ratio cavity between the fiber surface and the wall of the microcapillary pore. A model for the growth of the nanotubes within the capillary is demonstrated based on diffusion of the reactants and intermediates within the pore of the capillary and first order reaction kinetics on the surface of the fiber.

2. CNT-BASED ARTIFICIAL HAIR SENSORS

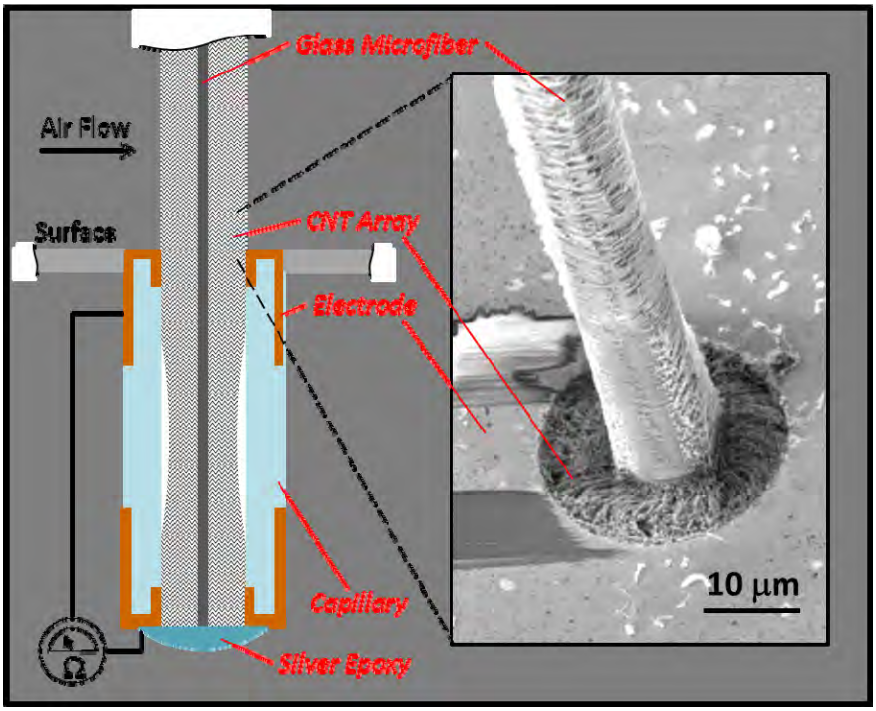

Figure 1. (Left) Cross-sectional schematic of nanotube-microfiber artificial hair sensor (not to scale). The alumina-coated glass microfiber hair is inserted into the glass capillary pore (with pre-deposited top and bottom electrodes) prior to CNT synthesis. The CNT array grows radially from the microfiber along its entire length, self-positioning the fiber at the center of the pore. After synthesis the fiber is affixed at the base of the capillary with silver epoxy. (Right) SEM image looking down at the top of the capillary opening. A focused ion beam was used to remove the CNTs from the fiber to expose the CNT array just inside the pore for imaging. When the fiber is deflected by the air flow, the CNT array at the opening is compressed against the capillary electrode changing the electrical resistance.

2.1 Device Fabrication

The CNT-on-fiber hair sensors are fabricated by a combination of hand-assembly, deposition, and growth processes (Figure 1). For the pore of the hair, a section of glass microcapillary of length L (typically 1 to 2 mm) and inner radius r_o (12.5 μm unless otherwise noted) is polished on the ends and coated on each end with chrome and gold by sputter deposition. Each metal electrode uniformly coats about 50 μm into the interior walls and is continuous out onto the polished ends and extends a few hundred microns down the exterior sides. The hair is a glass microfiber (AGY 933 S-2) of radius r_i = 4 μm coated with alumina by atomic layer deposition to promote nanotube growth. The fiber extends the full length of the capillary plus an additional external length L_E to be exposed to the air flow. The microfiber is inserted into the metalized capillary and the entire assembly is exposed to the nanotube growth process, the details of which are described in Section 3.

The nanotube array grows radially from the glass fiber surface both within and external to the capillary, self-positioning the fiber at the radial center of the capillary. The nanotube array also forms an electrical path between the two electrodes on the ends of the capillary. During operation of the sensor, the CNTs mechanically support the base of the fiber within the capillary. As the hair is deflected, the nanotubes near the pore opening are compressed against the electrode bringing the nanotubes into better contact with the metalized wall as well as increasing the local density of the array. This is detected as a drop in electrical resistance measured between the two ends of the capillary.

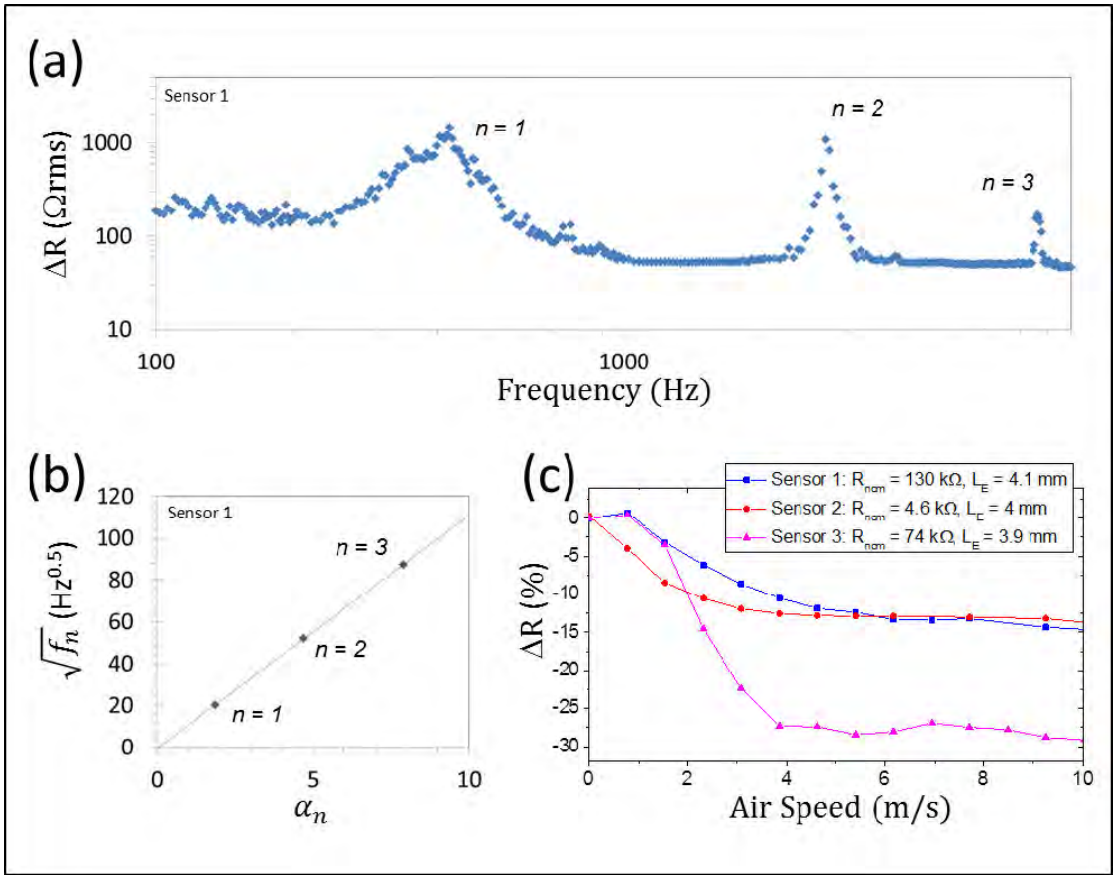

Figure 2. (a) The change in resistance of Sensor 1 in a plane wave tube to a sinusoidal air flow of varying frequency. The air flow is modulated by a speaker and the sound pressure maintained at a constant amplitude of 300 Pa as measured by a microphone directly above the sensor. Peaks in the resistance change are observed corresponding to the first three resonance modes of the hair. (b) The square root of the resonance frequencies f_n are observed to vary linearly with the scaling factor α_n as predicted for a fixed based Euler-Bernoulli cantilever beam. (c) The response of Sensor 1 and two additional sensors to varying static flow with noted external hair length (L_E) and nominal resistance. Sensor 2 has a steeper response at zero air velocity and Sensor 3 has an overall large magnitude of response.

2.2 Variable Deflection Response

A plane wave tube setup was used to determine the response of the sensors to both steady and oscillating air flows. A function generator sends a sinusoidal signal to a compression driver that modulates the air flow in the tube and a microphone above the hair sensor detects the resulting sound pressure. The RMS change in resistance of a typical sensor over a range of acoustic frequencies is shown in Figure 2a. A PID controller was used to adjust the driving signal such that the pressure was maintained at an amplitude of 300 Pa for all frequencies corresponding to an air velocity amplitude of about 0.5 m/s. The response is linear at low frequencies followed by three observed peaks corresponding to the first three resonance modes of the hair.

For a Euler-Bernoulli beam in bending, the natural resonance frequencies f_n are predicted to be

$$f_n = \frac{\alpha_n^2}{2\pi L_E^{\,2}}\sqrt{\frac{EI}{\rho A}} \tag{1}$$

where E is the Young's modulus, I is the moment of inertia, ρ is the density, and A is the cross-sectional area of the beam. The scaling factors α_n are determined from the boundary conditions. For a beam that is fixed at the base and free at the end, the first three α_n are 1.875, 4.694, and 7.854. The square root of the frequencies corresponding to the peaks can be seen to vary linearly with these scaling factors (Figure 2b) in agreement with a fixed base beam. This suggests that the stiffness of the nanotube array is large enough to greatly restrict the base of the fiber from deflecting. Since the resistance change should be proportional to this deflection, it may be possible to increase the response of the sensors by decreasing the stiffness of the array without impacting the bandwidth-limiting first resonance frequency.

The quasi-static responses of this sensor and two additional sensors to steady air flow inside the plane wave tube are shown in Figure 2c. The air speed was calculated from the pressure drop along the length of the plane wave tube[23]. To normalize the three sensors, the response is reported as a fractional change from the nominal resistance of the sensor at zero deflection. Sensors 1 and 3 show very little response at 1 m/s while the change in Sensor 2 is almost 5%. Sensors 1 and 2 are similar to each other as the air speed is further increased, approaching a change of about 12% at about 5 m/s and very little change thereafter. Sensor 3 displayed a steeper change in resistance with increasing air speed from 2 to 4

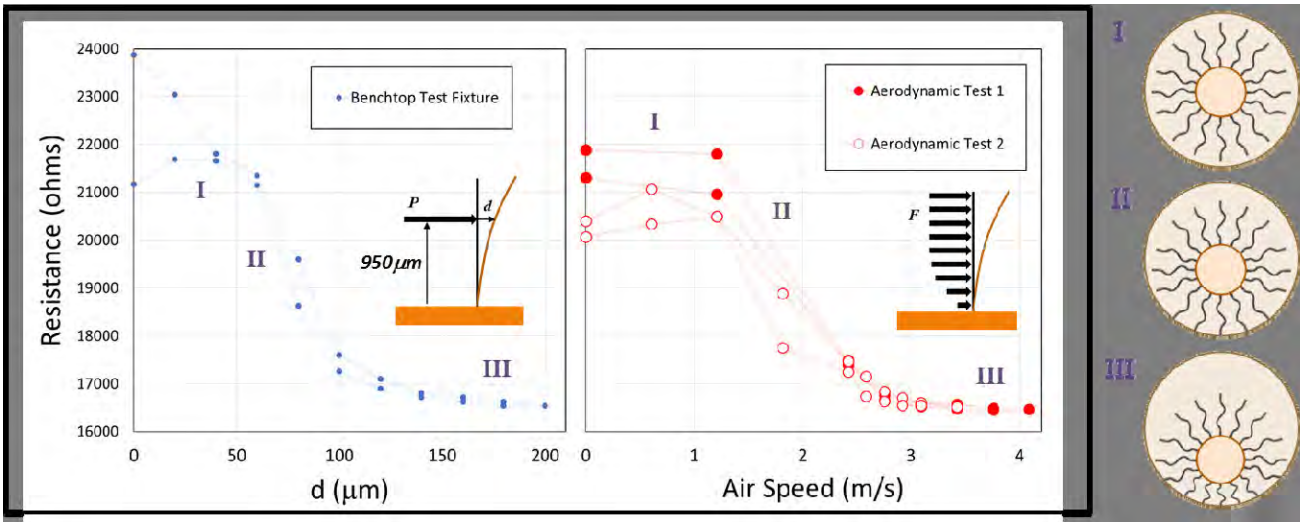

Figure 3. The response of Sensor 4 to a varying point load in a bench-top test fixture and the response of the same sensor to the distributed steady aerodynamic forces of air at varying velocities inside a plane wave tube. A schematic of the cross-section of the nanotube coated fiber at the capillary opening (large outer circle) is shown on the right. It is assumed that the nanotubes in this sensor do not quite fill the capillary opening resulting in little to no resistance change for small deflections of the hair (I). The largest change in resistance is observed just as the nanotubes come into contact with the metalized capillary wall (II). As the nanotube array begins to compress for large hair deflections (III), the observed resistance change is again small.

m/s, plateauing at about 27%. To quantitatively compare these and other sensors, we define the sensitivity as the ratio of the fractional resistance change to the change in air speed. Even comparing the response at the extremes of 0 and 10 m/s which includes much of the range where the sensitivity has significantly decreased, the values of 1.5%, 1.4%, and 2.9% per m/s for Sensors 1, 2 and 3, respectively, are higher than the sensitivities reported for other hair sensors (typically less than 0.1% per m/s)[21]. While the small, nonlinear quasi-static response of Sensor 1 near zero air velocity still results in a detectable response to oscillating air flows of amplitude below 1 m/s, the linear response of Sensor 2 near zero air velocity is more ideal for conventional operation. The differences between these CNT-based sensors in overall and low-flow sensitivity may be correlated to differences in the nanotube array profile between the fiber and capillary wall.

The response of a fourth sensor to quasi-static deflection by two methods is shown in Figure 3. Similar to Sensor 1, the change in response to varying air flow in the plane wave tube is nearly zero for air speeds up to about 1.2 m/s followed by a region of high sensitivity before plateauing at about 5 kΩ of total resistance change around 3 m/s. While this was for a distributed aerodynamic load, the same trend was observed in our point load bench-top test fixture. The change in the resistance was measured as the hair of the sensor was deflected by a distance d at a point 950 µm along the fiber from the capillary opening. The change in resistance was again near-zero for d up to 60 µm followed by large changes for increasing d up to about 120 µm. For larger deflections, the resistance of the sensor plateaus in a manner similar to that obtained during steady air flow.

The agreement between the tests suggests that the small air flows are successful in deflecting the hair even though no resistance change is observed, but the deflection is not electrically transduced by the nanotubes. We suggest the following explanation for the three regions of response, designated as I, II, and III on the plots with schematics of the cross-section of the device near the capillary opening shown to the right of Figure 3. Assuming the nanotube array is not quite tall enough to fill up the capillary at the opening, at small air flows (I) the fiber is deflected at the base but not enough to bring the nanotubes into contact with the metallized capillary wall. As the air speed is increased (II) the nanotubes are just brought into contact with one side of the capillary and the largest decrease in resistance is observed. At relatively high air speeds (III) the nanotube array is fully in contact with the electrode and further changes in resistance are dominated by local densification of the nanotube array. Likewise Maschmann et al. indicate from com-

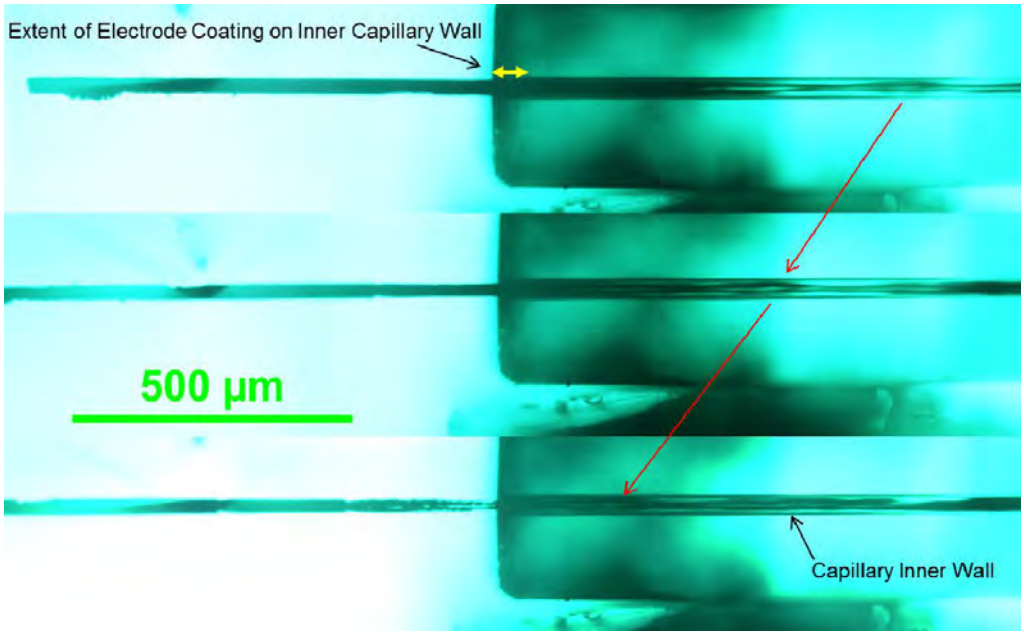

Figure 4. A back-lit optical image of a hair sensor looking at the exposed hair on the left and at the internal portion of the hair through the capillary on the right. The height of the nanotube array (or total CNT-glass diameter) is largely uniform along the length of the exposed hair. Inside the capillary, the nanotube array is of similar height at the opening of the capillary and reduced height toward the midpoint of the capillary. The top image shows the sensor as fabricated followed by images of the sensor after the hair has been shifted out of the capillary by 225 and 275 µm respectively (tracked by the arrows).

-pression measurements of planar CNT arrays that the resistance change is dominated by the CNT-electrode contact resistance over the changes to the bulk[24]. If these assumptions are correct, sensors having slightly longer CNTs of sufficient length to contact the electrode walls prior to deflection would initially respond with the sensitivity of region II. A sensor with an even taller nanotube array – such that the array is in pre-compression prior to deflection – would initially resemble the compressed array of region III, showing little response to deflection.

An optical image of a fifth sensor is shown Figure 4. The image is back lit through the transparent capillary such that the nanotube coated hair is visible both outside and inside the capillary. The nanotube array is highly optically absorbing and appears black in the image. But where the nanotubes are short or are not present, the nanotube-coated glass fiber is transparent. The nanotube height is fairly constant outside the capillary with a total nanotube-glass-fiber diameter of about 25 μm. Inside the capillary the nanotube array is of similar height near the opening, but the nanotubes are shorter toward the axial middle of the capillary. This is expected and will be discussed further in Section 3.

The top image shows the sensor as fabricated followed by images of the sensor after the hair has been shifted out of the capillary in two increments. In each case the hair was then deflected by 100 μm by a point load applied 530 μm from the capillary opening and the change in resistance measured. In the as-grown sensor, the nanotubes fill up the capillary opening and the change in resistance was less than 0.5%. Since the nanotubes were slightly overgrown, they experience little change to the nanotube-electrode connection and only changes in the bulk compression. In the second image the nanotube-fiber diameter is at or slightly less than the inner diameter of the capillary. The nanotube array is not as dense near the electrode initially resulting in a large 7% change in resistance as the fiber was deflected. In the third image the shortest nanotube array is within the metallized portion of the capillary and no resistance change was observed at this magnitude of deflection. At the capillary opening the deflection of the base of the fiber is not large enough to bring the nanotube array into contact with the capillary wall. Better understanding of the onset of the high sensitivity response will enable optimization of the sensors through control of the parameters that govern nanotube growth inside the capillary.

3. CNT ARRAY SYNTHESIS IN HIGH ASPECT RATIO MICROCAVITIES

Growing the nanotube array to an optimum height at the pore opening was emphasized in the previous section, and here we show how that height is related to the length of the nanotubes within the capillary. As mentioned previously, the nanotubes near either opening of the capillary are almost as long as the nanotubes on the fiber external to the capillary but are shorter near the axial center. This difference is increased with a longer capillary length. This is consistent with the reactive gases diffusing into the capillary from the ends while consumed at the surface of the fiber and converted into nanotubes, decreasing their concentration towards the middle of the capillary. For these sensors, the nanotubes inside the capillary provide the mechanical support to the fiber within the capillary and are the electrical connection between the two ends of the sensor. A short nanotube array will have a higher nominal resistance, and a long enough capillary will be an open circuit due to regions of no nanotube growth. While this application pushes towards continuity of the nanotube array within the capillary, it may be possible to use this restricted growth to realize tapered microstructures such as tailored hair shapes, micro-antennae, brushes, or filters.

The CNT arrays are synthesized in a 1” diameter quartz tube furnace reactor by a liquid injection method at atmospheric pressure[25]. The alumina coated fibers are inserted into the capillaries and multiple devices are placed on a graphite carrier substrate inside the tube furnace perpendicular to the direction of gas flow. Argon and hydrogen are flowed through the tube at 50 and 500 sccm respectively as the sample is heated from room temperature to 750 ^{o}C and continuing during synthesis. Once the growth temperature is achieved, a 5% by weight liquid mixture of ferrocene suspended in xylene is injected continuously at a rate of 2 ml/hr into the tube furnace near the opening where the temperature is about 200 ^{o}C. The gaseous products of the ferrocene/xylene vaporization flow with the Ar/H_2 gases to the devices. During the duration of the growths here, the nanotubes grow nearly exclusively on the alumina coated surface of the glass fibers. The iron from the ferrocene forms iron nanoparticles on the growth surface, each of which support the growth of a single multiwalled nanotube with additional carbon material added at the iron nanotube interface (e.g. base growth). The nanotubes grow along the surface until a sufficient number are present to support lift-off. From there the nanotubes grow as a partially entangled forest or array primarily aligned vertically from the surface (radially from the fiber). The radial height of the array (h) is similar to but less than the length of the individual CNT lengths since the

CNTs are wavy within the array. The nanotube array can be considered as a bulk material with density ρ_{CNT}. It is foam-like in its mechanical behavior[13, 15, 26, 27] and about 3% dense by volume[28, 29].

Our model for the growth of the nanotubes within the capillary is based on diffusion of the reactants and intermediates within the pore of the capillary and first order reaction kinetics on the surface of the alumina coated glass fiber. While the xylene and ferrocene mixture is generally assumed to break down into many reactive species at nanotube growth temperatures[25, 30], we are concerned with the average behavior of the system. Therefore we consider a single diffusion coefficient (D_{eff}) and a single reaction coefficient (k''). This average or effective diffusion coefficient gives the binary diffusive transport of the average reactive species relative to the remaining gases considered as a whole. The average reactive species is modeled to be consumed at the surface of the fiber by a first order reaction at a rate proportional to the reaction coefficient k''. The double prime follows the typical notation for a surface reaction with units of cm s^{-1}. The identity of this species is not the focus here but rather how these diffusive and reactive processes work together to determine the CNT array profile within the capillary.

Outside the capillary, the concentration of the reactive species (c) is assumed to be constant and the height of the nanotube array (h) measured from the surface of the fiber is simply given by

$$h = \frac{ck''t}{\rho_{CNT}} \tag{2}$$

where t is the reaction time and ρ_{CNT} is the density of the nanotube array. Inside the capillary at any given time, the concentration varies down the length of the capillary and radially from the fiber surface. We make a second approximation to further simplify the model that the radial variation in concentration is negligible compared to the axial variation. In this case the system can be modeled as a one dimensional system in which the reaction at the surface can be thought of as existing throughout the open volume in the capillary. This volumetric reaction is proportional to the constant k''' with units of s^{-1} and is related to the surface reaction constant by the ratio of the area of the reactive surface to the volume of the enclosed cavity:

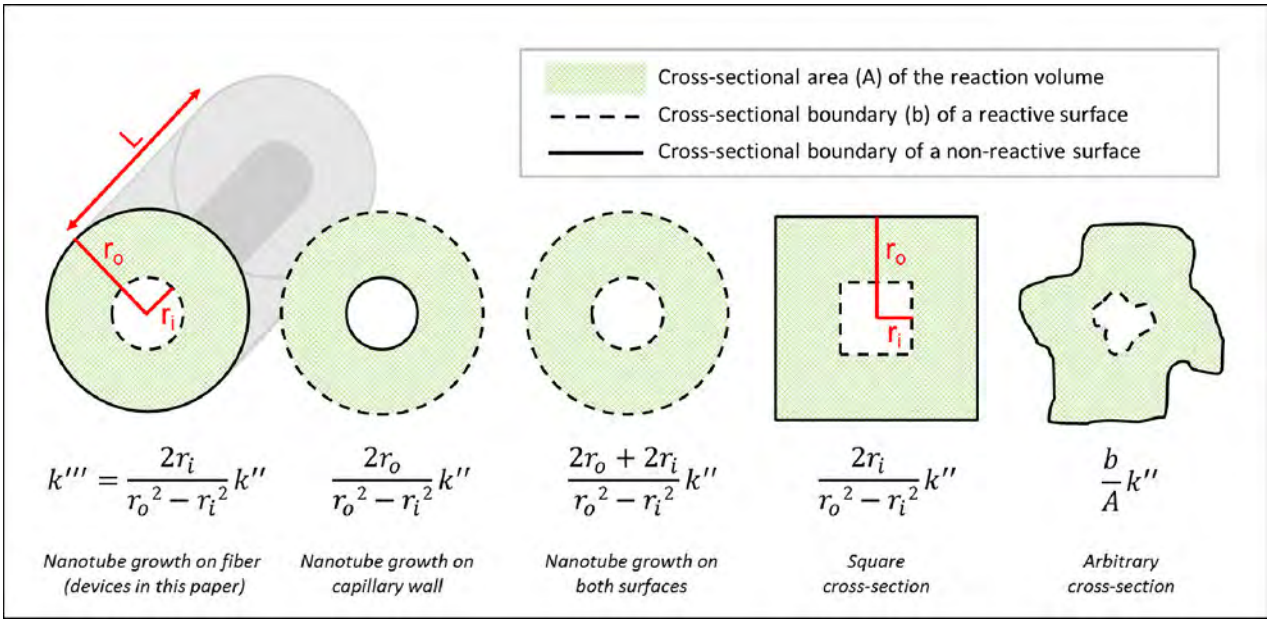

Figure 5. A schematic of the glass fiber inside the capillary of length L is shown on the left. The open space between the fiber and capillary form a high aspect ratio tube for gas flow with cross section A (hashed green) between two circles of inner radius r_i (the fiber radius) and out radius r_o (the capillary radius). The nanotubes only grow on the alumina coated glass fiber, so the cross-sectional length of the perimeter of the fiber is the reactive boundary b. The surface rate of reaction is proportional to the reaction constant k'' and can be approximated as a homogeneous, volumeric reaction with reaction constant bk''/A or k'''. The relationship between k'' and k''' is shown for these devices as well as tubes differing in cross-section or combination of reactive boundaries (dashed line) and un-reactive boundaries (solid lines).

$$k''' \approx \frac{A_{reactive}}{V_{enclosed}} k'' = \frac{b}{A} k''. \tag{3}$$

Since the reactive area and enclosed volume share the same axial length L, the relationship reduces to the ratio of the cross-sectional perimeter of the reactive surface (b) and the cross-sectional area (A) of the enclosed volume. For the devices here, A is the cross-section of the open space between the capillary wall (radius r_o) and the fiber (radius r_i) – or $\pi r_0^2 - \pi r_i^2$ – and b is the length around the perimeter of the alumina coated fiber $2\pi r_i$ since nanotubes do not grow on the capillary wall (Figure 5). It can also be seen in Figure 5 that this relationship will hold for any tube with continuous axial cross-section taking into account the total reactive boundary. While the surface reaction constant k'' is independent of the dimensions of the system, the reaction constant for the projected volume k''' is expected to scale as the cross-section (e.g. capillary radius) is changed.

Assuming the effective diffusion coefficient and volumetric reaction constants do not change with time or concentration, the concentration profile inside the capillary is modeled by Fick's law in one dimension:

$$\frac{\partial c(y,t)}{\partial t} = D_{eff} \frac{\partial^2 c(y,t)}{\partial y^2} - k''' c(y,t). \tag{4}$$

The boundary conditions are similar to a classic Stefan diffusion tube[31, 32]: the reactive species concentration at the openings of the capillary is assumed to remain constant throughout the reaction and zero inside the capillary at the start of the reaction. Since the concentration is constant, the height of the nanotubes at the opening is given by Equation 2. We find that the nanotube array height at the openings is not the same from sample to sample, so we assume the external concentration to vary spatially inside the growth furnace but remain constant in time. In this case each end of the capillary experiences a unique constant concentration boundary condition, c_1 and c_2, and the solution to Equation 4 can be separated for the two openings:

$$c(y,t) = c_1 f_1(D_{eff}, k''', L, y, t) + c_2 f_2(D_{eff}, k''', L, y, t). \tag{5}$$

The height of the nanotube array after synthesis can be measured inside and outside the capillary and is found from the model by integrating the concentration profile in the previous equation:

$$h(y,t) = \frac{c_1 k''}{\rho_{CNT}} \int_0^t f_1(D_{eff}, k''', L, y, t) dt + \frac{c_2 k''}{\rho_{CNT}} \int_0^t f_2(D_{eff}, k''', L, y, t) dt. \tag{6}$$

Using Equation 2, the unknown concentration, density, and surface reaction rate are replaced with the measured CNT heights at the openings h_1 and h_2:

$$h(y,t) = \frac{h_1}{t} F_1(D_{eff}, k''', L, y, t) + \frac{h_2}{t} F_2(D_{eff}, k''', L, y, t). \tag{7}$$

To test the model, nanotubes were grown on fibers in capillaries of five different lengths and two different radii (r_o = 12.5 and r_o = 20 um) during the same growth run for a duration t of 180 s. The resulting nanotube height profiles are shown versus axial position in Figure 6. While not smooth, the height profile is observed to be larger at the ends of the capillary than in the interior as expected from the assumptions about the system, and this difference is more pronounced with increasing capillary length. What is more, the nanotube array is not continuous from end to end in the two longest devices; these devices would be non-functioning since there is no continuous axial path for the current even though the nanotubes are the ideal height at the openings. It can also be seen that the axial position of the height minimum is shifted towards the end of the capillary with the shorter nanotubes – e.g. Devices C and E – as expected for a difference in source concentration between the ends. Perhaps harder to distinguish by eye, the nanotube growth is less in the capillaries with smaller radii. In example, the near-zero-growth regions of the Device E are much smaller than Device D even though the capillary is slightly longer. Note that the model does not account for any spatial heterogeneity of the growth that might be caused by non-uniform catalyst distribution or variation in growth efficiency.

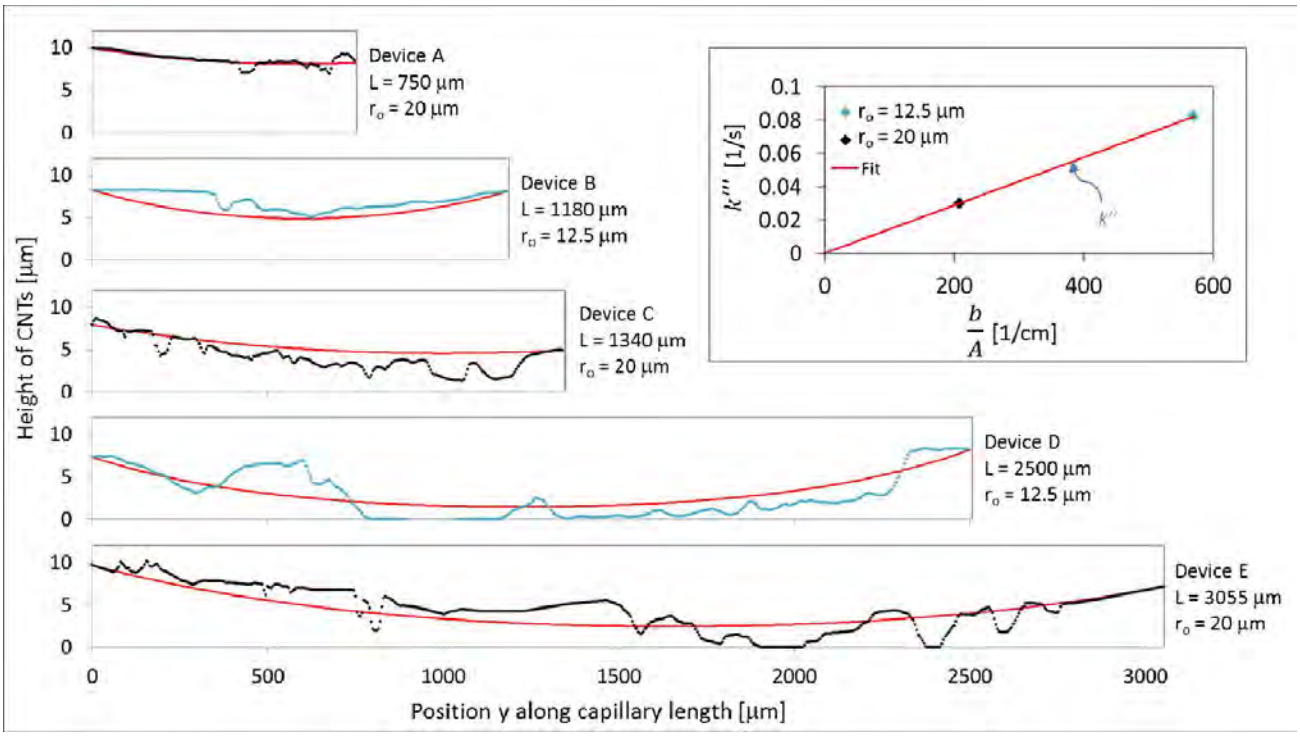

Figure 6. The height of nanotube arrays grown vertically from the surface of alumina coated glass fibers of radius 4 µm inside capillaries of two different inner radii (r_o) and five different lengths as noted. The time of the growth was 180 s. The red curves are the best fits to the model based a Fick's law with an average diffusion constant D_{eff} and an approximate volumetric reaction rate k''' scaled by the dimensions of the system to the surface reaction rate k''. The predicted profiles are the same and the R^2 is a maximum of 0.9254 for all $D_{eff} \geq 0.00025$ cm^2/s. (inset) In example for $D_{eff} = 0.00025$ cm^2/s, the best fit values for k''' for the two capillary radii scale linearly as expected with the ratio of the reactive cross-section perimeter b and the cross-sectional area of flow A. The slope corresponds to a k'' of 0.00014 cm/s at this D_{eff}.

Equation 7 was fit against all five of the nanotube growth profiles with $k_{12.5}'''$, k_{20}''', and D_{eff} as the 3 fit parameters where the subscripts on k''' designate the value of r_o in µm. Even though the model can only predict a smooth profile, the resulting predicted height profiles (Figure 6 red curves) fit the measured profiles with a coefficient of determination R^2 of 0.9254, affirming the assumptions of our model for this confined geometry. For the predicted profiles in this image, D_{eff} is 0.00025 cm^2 s^{-1} and the corresponding diffusion length $(tD_{eff})^{1/2}$ is 0.21 cm. The k''' are plotted against the ratio $2r_i/(r_o^2-r_i^2)$ per Equation 3 (Figure 6 inset). In agreement with the assumption of negligible radial concentration variation, the two k''' are seen to scale linearly and correspond to a k'' of 0.00014 cm s^{-1}.

Plotting the R^2 from the fit versus the diffusion coefficient, it is seen that the R^2 increases up to a maximum of 0.9254 at $D_{eff} = 0.00025$ cm^2 s^{-1} but plateaus rather than coming to a peak (Figure 7). The fit is just as good for all larger values of D_{eff}, suggesting that the values determined previously are the minimum possible values for D_{eff} and k''. Likewise, the reaction constant k'' corresponding to the best fit increases nonlinearly with D_{eff} up to the best-fit minimum D_{eff} but approximately linearly thereafter. The CNT height profile appears to be uniquely dependent on the ratio of k'' to D_{eff} but not on either value alone.

Looking again at the model, both the non-dimensional functions f in the concentration profile in Equation 5 have a time-independent, steady-state (SS) component and a transient (T) component

$$f(y,t) = f_{SS}(y) + f_T(y,t) \tag{8}$$

such that the integrated functions F in Equation 7 are likewise

$$F(y,t) = tf_{SS}(y) + F_T(y,t). \tag{9}$$

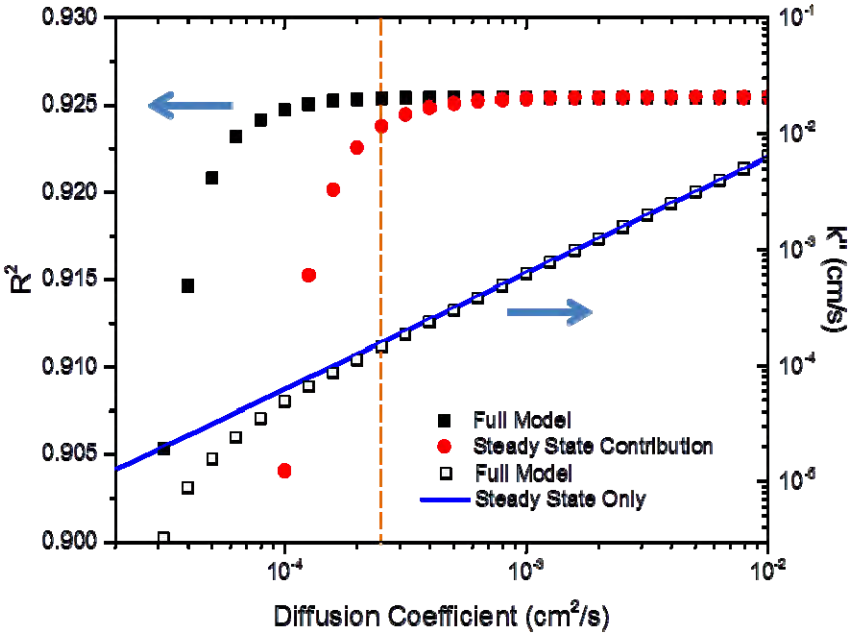

Figure 7. The coefficient of determination R^2 of the fit of the model to the measured CNT height profiles and the k" corresponding to the best fit k''' parameters versus the effective diffusion coefficient D_{eff}. The R^2 is maximized at 0.9254 and the k" is linear for all D_{eff} greater than 0.00025 $cm^2\ s^{-1}$ marked with a dashed line. The red circles show the fit to be almost as good using the same k''' and D_{eff} from the full model but excluding the transient terms when calculating the predicted profiles. The blue line marks the k'' found from the best fit to the model only considering the steady state terms. For the times required to grow the CNTs to fill the cross section at the opening, the reactive species concentration is at steady state over most of the growth duration and the resulting height profile can be determined from the ratio of k'' to D_{eff} found to be 0.624 cm^{-1} under these growth conditions.

The steady state component for the first end is given by

$$f_{SS,1}(y) = \sinh\left((L-y)\sqrt{\frac{k'''}{D_{eff}}}\right) \Big/ \sinh\left(L\sqrt{\frac{k'''}{D_{eff}}}\right), \tag{10}$$

and $f_{SS,2}(y)$ has the same form with the L-y replaced by y. While the dependence of the transient component on the reaction rate and diffusion coefficient is complex (not shown), the steady-state component of f is dependent purely on the ratio of the two parameters.

Two analyses were performed to investigate the role of this ratio and steady state component. First, the data was fit against Equation 7 but with the transient term (F_T in Equation 9) set to zero. In this scenario the system reaches steady state instantaneously, approximately equivalent to the system reaching steady state quickly relative to the total growth time. The two ratios k'''/D_{eff} served as the two fit parameters which in turn were used to determine k''/D_{eff}. The R^2 of the best fit is again 0.9254 corresponding to a k''/D_{eff} of 0.624 cm^{-1}. Plotting a line with this slope in Figure 7, it can be seen that this ratio matches the slope of the linear k'' relationship to D_{eff} predicted by the full model.

The steady-state contribution was also assessed by calculating R^2 versus D_{eff} with the transient term again set to zero but with the values of $k_{12\,5}'''$ and k_{20}''' previously determined from the best fit using the full model. For low values of the diffusion coefficient, the system takes longer to reach steady state and the transient terms have a larger impact on the quality of fit. But as D_{eff} increases above 0.00025 $cm^2\ s^{-1}$ the steady state term dominates with a fit as good as the full model as indicated by the same R^2 for all but the lowest values of D_{eff}. For synthesis of a nanotube array that nearly fills the cross section at the openings, we conclude from these two results that the concentration profile of the reactive species

along the length of the capillary is at steady state over most of growth period. Under these steady state conditions the shape of the height profile is primarily determined by the ratio of k'' to D_{eff}.

Substituting k'' for k''' in $f_{SS}(y)$ using Equation 3 and moving the L under the square root, it can be seen that the height profile determined from the steady state concentration depends on the product of the two dimensionless ratios Lb/A and Lk''/D_{eff}. The first is essentially the physical aspect ratio of the system taking into account the relative scale of the reactive surface. In the field of fluid flow, A/b is referred to as the hydraulic radius where b is instead the wetted perimeter and the flow velocity increases with increased hydraulic radius. D_{eff}/k'' also has units of length and can be thought of as the ability of the reactive species to move axially by diffusive forces against the competing reaction flux. Dividing the length by this value gives a dimensionless quantity referred to here as the chemical aspect ratio.

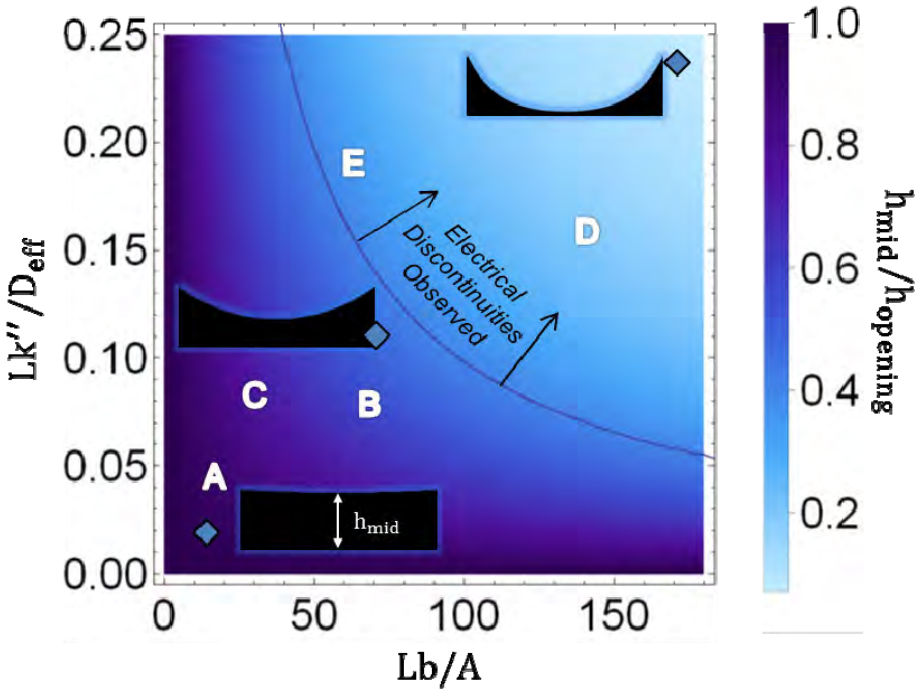

Figure 8. The predicted nanotube array height – or total reaction product – at the midpoint per the nanotube height at the opening of a high aspect ratio tube versus the physical aspect ratio Lb/A and chemical aspect ratio Lk''/D_{eff} from a steady state concentration profile. The white letters mark the values for the five devices characterized in this section. Using the values corresponding to the diamonds, three example height profiles with constant L are shown as insets ranging from nearly uniform along the length of the tube for lower values of the physical and chemical aspect ratios to highly tapered for larger aspect ratios. It is estimated based on experimental observations that regions of no growth (electrically discontinuous) occur when the predicted midpoint height is below about 40% of the height at the opening (marked as a line on the graph). Sensors above and to the right of this line are expected to have a high likelihood of being electrically discontinuous along the axial and of limited use for this applications.

To show the relative impact of these factors in high aspect ratio reaction volumes, the predicted height of the nanotube array at the axial midpoint relative to the unrestricted height at the openings under steady state concentration conditions is plotted against a range of physical and chemical aspect ratios in Figure 8. For this calculation the constant reactive species concentrations at the two openings c_1 and c_2 were assumed to be equal. In general this height is equivalent to a measure of the total chemical surface reaction due to the reduced concentration inside the reaction volume relative to the total reaction that would take place over the same time period with the full source concentration. The five devices of Figure 6 are shown as well as 3 example length-normalized profiles. For low values of the ratios the total reaction profile is seen to be nearly constant long the axial length and the angle between the side and top of the profile is nearly $\pi/2$. As either ratio is increased, the height at the midpoint and the angle at the opening decrease ultimately resulting in a highly tapered profile.

In the specific case of the artificial hair sensors, the axial resistance will be minimized for minimized capillary length and maximized h_{mid} corresponding to low physical and chemical aspect ratios. A uniform nanotube array profile also corresponds to a more uniform elastic support for the hair within the capillary. But for purposes such as handling it is often desirable to maximize the capillary length while at least maintaining electrical continuity. As hinted in the discussion about the sensor operation, it may also be desirable to reduce the stiffness of the nanotube support to increase the deflection of the hair inside the capillary near the electrode at the opening. This may be achieved by reducing the quantity of nanotubes such as from a highly tapered profile. While the model will never predict a zero height that would correspond to an electrical break, we observe regions of no nanotube growth when the predicted height at the midpoint is lower than about 40% of the opening height. This line is marked in Figure 8 and corresponds to the longest capillary and highest degree of taper possible while maintaining axial electrical continuity.

4. CONCLUSIONS

Within this paper we have described the operation of a simple, yet sensitive artificial hair air flow sensor whose performance can be tailored by changing the dimensions of the capillary used, the CNT growth conditions, and axially displacing the hair within the capillary. The CNT synthesis on the fiber within a capillary can be modeled and used to tailor the degree of taper of the CNT profile along the length of the fiber and within the capillary. The behavior of the sensors is described in terms of three regions – (I) a region in which the hair is mechanically moved, but not yet sufficiently compressed to result in a change in electrical resistance, (II) a highly sensitive region in which the CNT array is initially coming into contact with the electrode and starting to compress such that the electrical resistance decreases significantly, and (III) a region in which the CNTs continue to be compressed but the electrical sensitivity begins to saturate. Strong correlation between point-loaded lab deflection experiments and distributed deflection under steady state flow was observed. Overall, the stiffness of the nanotube array is large enough to greatly restrict the base of the fiber from deflecting which indicates it may be possible to further enhance the response of the sensors by decreasing the stiffness of the CNT array or changing the axial profile of the CNT array. One can envision tailored, non-evasive arrays of air flow sensors optimized for a given application. The ability to tailor the response of these sensors when coupled with their small size, ease of integration, and simple operation, has the potential to also enable a large variety of sensors beyond air flow sensors.

REFERENCES

[1] J. A. C. Humphrey, R. Devarakonda, I. Iglesias *et al.*, [Dynamics of Arthropod Filiform Hairs. I. Mathematical Modelling of the Hair and Air Motions], (1993).

[2] C. Magal, O. Dangles, P. Caparroy *et al.*, "Hair canopy of cricket sensory system tuned to predator signals," Journal of Theoretical Biology, 241(3), 459-466 (2006).

[3] J. M. Camhi, "Locust Wind Receptors: I. Transducer Mechanics and Sensory Response," Journal of Experimental Biology, 50(2), 335-348 (1969).

[4] S. Sterbing-D'Angelo, M. Chadha, C. Chiu *et al.*, "Bat wing sensors support flight control," Proceedings of the National Academy of Sciences, 108(27), 11291-11296 (2011).

[5] C. Brent, W. Stephen, Edward Haering, Jr. *et al.*, [Flush airdata sensing (FADS) system calibration procedures and results for blunt forebodies] American Institute of Aeronautics and Astronautics, (1999).

[6] B. T. Dickinson, J. R. Singler, and B. A. Batten, "Mathematical modeling and simulation of biologically inspired hair receptor arrays in laminar unsteady flow separation," Journal of Fluids and Structures, 29(0), 1-17 (2012).

[7] H. Shen, Y. Xu, and B. T. Dickinson, "Fault tolerant attitude control for small unmanned aircraft systems equipped with an airflow sensor array," Bioinspiration & Biomimetics, 9(4), 046015 (2014).

[8] T. Junliang, and Y. Xiong, "Hair flow sensors: from bio-inspiration to bio-mimicking—a review," Smart Materials and Structures, 21(11), 113001 (2012).

[9] R. M. Matthew, D. Ben, J. E. Gregory *et al.*, "Force sensitive carbon nanotube arrays for biologically inspired airflow sensing," Smart Materials and Structures, 21(9), 094024 (2012).

[10] G. J. Ehlert, M. R. Maschmann, and J. W. Baur, "Electromechanical behavior of aligned carbon nanotube arrays for bio-inspired fluid flow sensors." 7977, 79771C-79771C-15.

[11] SuhrJ, VictorP, CiL *et al.*, "Fatigue resistance of aligned carbon nanotube arrays under cyclic compression," Nat Nano, 2(7), 417-421 (2007).
[12] M. C. McCrary-Dennis, and O. I. Okoli, "A review of multiscale composite manufacturing and challenges," Journal of Reinforced Plastics and Composites, 31(24), 1687-1711 (2012).
[13] M. R. Maschmann, G. J. Ehlert, S. Tawfick *et al.*, "Continuum analysis of carbon nanotube array buckling enabled by anisotropic elastic measurements and modeling," Carbon, 66(0), 377-386 (2014).
[14] M. R. Maschmann, G. J. Ehlert, S. J. Park *et al.*, "Visualizing Strain Evolution and Coordinated Buckling within CNT Arrays by In Situ Digital Image Correlation," Advanced Functional Materials, 22(22), 4686-4695 (2012).
[15] M. R. Maschmann, Q. Zhang, R. Wheeler *et al.*, "In situ SEM Observation of Column-like and Foam-like CNT Array Nanoindentation," ACS Applied Materials & Interfaces, 3(3), 648-653 (2011).
[16] M. Bedewy, B. Farmer, and A. J. Hart, "Synergetic Chemical Coupling Controls the Uniformity of Carbon Nanotube Microstructure Growth," ACS Nano, 8(6), 5799-5812 (2014).
[17] P. B. Amama, C. L. Pint, L. McJilton *et al.*, "Role of Water in Super Growth of Single-Walled Carbon Nanotube Carpets," Nano Letters, 9(1), 44-49 (2008).
[18] A. A. Puretzky, D. B. Geohegan, S. Jesse *et al.*, "In situ measurements and modeling of carbon nanotube array growth kinetics during chemical vapor deposition," Applied Physics A, 81(2), 223-240 (2005).
[19] G. Ehlert, M. R. Maschmann, and J. Baur, "Morphology control in hierarchical fibers for applications in hair flow sensors."
[20] N. Yamamoto, A. John Hart, E. J. Garcia *et al.*, "High-yield growth and morphology control of aligned carbon nanotubes on ceramic fibers for multifunctional enhancement of structural composites," Carbon, 47(3), 551-560 (2009).
[21] M. R. Maschmann, G. J. Ehlert, B. T. Dickinson *et al.*, "Bioinspired Carbon Nanotube Fuzzy Fiber Hair Sensor for Air-Flow Detection," Advanced Materials, 26(20), 3230-3234 (2014).
[22] D. M. Phillips, K. A. Slinker, C. W. Ray *et al.*, "Artificial Hair Sensors: Electro-Mechanical Characterization," V002T06A016 (2014).
[23] V. Chandrasekaran, [Dynamic calibration technique for thermal shear-stress sensors with variable mean flow] University of Florida, Gainesville, FL(2000).
[24] M. R. Maschmann, B. Dickinson, G. J. Ehlert *et al.*, "Force sensitive carbon nanotube arrays for biologically inspired airflow sensing," Smart Materials and Structures, 21(9), 094024 (2012).
[25] R. Andrews, D. Jacques, A. M. Rao *et al.*, "Continuous production of aligned carbon nanotubes: a step closer to commercial realization," Chemical Physics Letters, 303(5–6), 467-474 (1999).
[26] A. Cao, P. L. Dickrell, W. G. Sawyer *et al.*, "Super-Compressible Foamlike Carbon Nanotube Films," Science, 310(5752), 1307-1310 (2005).
[27] M. R. Maschmann, Q. Zhang, F. Du *et al.*, "Length dependent foam-like mechanical response of axially indented vertically oriented carbon nanotube arrays," Carbon, 49(2), 386-397 (2011).
[28] X. Li, L. Ci, S. Kar *et al.*, "Densified aligned carbon nanotube films via vapor phase infiltration of carbon," Carbon, 45(4), 847-851 (2007).
[29] D. N. Futaba, K. Hata, T. Namai *et al.*, "84% Catalyst Activity of Water-Assisted Growth of Single Walled Carbon Nanotube Forest Characterization by a Statistical and Macroscopic Approach," The Journal of Physical Chemistry B, 110(15), 8035-8038 (2006).
[30] H. Endo, K. Kuwana, K. Saito *et al.*, "CFD prediction of carbon nanotube production rate in a CVD reactor," Chemical Physics Letters, 387(4–6), 307-311 (2004).
[31] J. Stefan, "Uber Einige Probleme der Theorie der Warmeleitung," S.-B. Wien-Akad. Mat. Natur., 98, 173-184 (1889).
[32] R. Carty, and T. Schrodt, "Concentration Profiles in Ternary Gaseous Diffusion," Industrial & Engineering Chemistry Fundamentals, 14(3), 276-278 (1975).